

UC Davis

UC Davis Previously Published Works

Title

Coupled Cluster Characterization of 1-, 2-, and 3-Pyrrolyl: Parameters for Vibrational and Rotational Spectroscopy

Permalink

<https://escholarship.org/uc/item/0wr4r852>

Journal

The Journal of Physical Chemistry A, 125(5)

ISSN

1089-5639

Authors

Johansen, Sommer L
Xu, Zhongxing
Westerfield, JH
[et al.](#)

Publication Date

2021-02-11

DOI

10.1021/acs.jpca.0c09833

Peer reviewed

Coupled Cluster Characterization of 1-, 2-, and 3-Pyrrolyl: Parameters for Vibrational and Rotational Spectroscopy

Sommer L. Johansen, Zhongxing Xu, J. H. Westerfield, Anna C.
Wannenmacher, and Kyle N. Crabtree*

*Department of Chemistry, University of California, Davis, One Shields Ave., Davis, CA
95616 USA*

E-mail: kncrabtree@ucdavis.edu

Abstract

Pyrrolyl (C_4H_4N) is a nitrogen-containing aromatic radical that is a derivative of pyrrole (C_4H_5N) and is an important intermediate in the combustion of biomass. It is also relevant for chemistry in Titan’s atmosphere and may be present in the interstellar medium. The lowest-energy isomer, 1-pyrrolyl, has been involved in many experimental and theoretical studies of the N–H photodissociation of pyrrole, yet it has only been directly spectroscopically detected via electron paramagnetic resonance and through the photoelectron spectrum of the pyrrolide anion, yielding three vibrational frequencies. No direct measurements of 2- or 3-pyrrolyl have been made, and little information is known from theoretical calculations beyond their relative energies. Here, we present an ab initio quantum chemical characterization of the three pyrrolyl isomers at the CCSD(T) level of theory in their ground electronic states, with an emphasis on spectroscopic parameters relevant for vibrational and rotational spectroscopy. Equilibrium geometries were optimized at the CCSD(T)/cc-pwCVTZ level of theory, and the quadratic, cubic, and partial quartic force constants were evaluated at CCSD(T)/ANO0 for analysis using second-order vibrational perturbation theory to obtain harmonic and anharmonic vibrational frequencies. In addition, zero-point-corrected rotational constants, electronic spin-rotation tensors, and nuclear hyperfine tensors are calculated for rotational spectroscopy. Our computed structures and energies agree well with earlier density functional theory calculations, and spectroscopic parameters for 1-pyrrolyl are compared with the limited existing experimental data. Finally, we discuss strategies for detecting these radicals using rotational and vibrational spectroscopy on the basis of the calculated spectroscopic constants.

Introduction

The study of nitrogen-containing heterocycles in the gas phase is important for combustion chemistry, astrochemistry, and the study of planetary atmospheres. Pyrrole (C_4H_5N), a

five-membered aromatic ring with one nitrogen, is present in fuels derived from biomass, including coal and biofuels.^{1,2} Pyrrole combustion leads to the formation of NO_x species and potentially nitrogen-containing polycyclic aromatic hydrocarbons (PAHs), both presenting health hazards.³⁻⁶ N-heterocycles, including pyrrole derivatives, have also been identified on meteorites with nonterrestrial isotopic abundances,⁷ and although no such molecule has been detected in space to date,⁸⁻¹⁰ numerous experimental studies of interstellar ice analogues under irradiation have produced these compounds.¹¹⁻¹⁴ In Titan’s atmosphere, nitrogen-containing hydrocarbons have been detected by radio astronomy¹⁵ and the Cassini ion neutral mass spectrometer (INMS),¹⁶⁻¹⁸ with a tentative INMS detection of pyrrole.

In each of these environments, radical intermediates play key roles in driving important chemical pathways. In interstellar clouds, for example, the barrierless reaction of the CN radical with benzene has been suggested to explain the recent detection of benzonitrile,^{19,20} and the aforementioned ice studies are strongly suspected to involve radical intermediates.¹⁴ Radical-mediated chemistry is also widely used in models of Titan’s atmosphere,²¹ and the potential for the presence of pyrrolyl ($\text{C}_4\text{H}_4\text{N}$), the radical derivative of pyrrole, has recently been explored.²² Finally, models of biofuel combustion explicitly depend on reactions involving the 1-pyrrolyl radical.²³⁻²⁹ Pyrrolyl has three isomeric forms: the 1-pyrrolyl radical that arises from N–H bond fission in pyrrole, and the 2- and 3-pyrrolyl radicals that come from the two possible C–H bond fission sites.

As the product of N–H photodissociation, 1-pyrrolyl has the subject of several experimental³⁰⁻³⁵ and theoretical studies³⁶⁻⁴¹ owing to its complex dynamics. The potential energy surface shows that along the N–H dissociation coordinate, pyrrole in its 1A_1 ground electronic state correlates to the 2A_1 second excited electronic state of 1-pyrrolyl, while the 2A_2 ground state of 1-pyrrolyl correlates to the 1A_2 excited electronic state of pyrrole. During photodissociation, population between these states is redistributed on the femtosecond time scale via a conical intersection.^{33,37} Photoexcitation of pyrrole to its 1B_2 electronic excited

state has also been found to yield 2- and/or 3-pyrrolyl via C–H bond fission following relaxation to vibrationally excited levels in the 1A_1 ground state, albeit on a slower time scale than N-H bond dissociation.^{30,33}

Despite numerous photochemistry experiments, direct spectroscopic observations of the pyrrolyl radicals are limited to only a few observations of 1-pyrrolyl. Three vibrational frequencies of 1-pyrrolyl were experimentally measured in the photoelectron spectrum of the pyrrolide anion.⁴² Several vibrational transitions were also attributed to 1-pyrrolyl in H Rydberg photofragmentation studies of pyrrole on the basis of density functional theory (DFT) calculations,³¹ but there is some ambiguity in the assignments. An electron spin resonance study of 1-pyrrolyl suggests that its unpaired electron is delocalized among the aromatic π bonds.⁴³ Information on 2- and 3-pyrrolyl is even more scarce. Two recent computational studies show that, unlike 1-pyrrolyl, they are σ -type radicals, with the unpaired electron localized to the respective carbon.^{22,44} These studies also included equilibrium geometries and the relative electronic energies of the three isomers.

Here, we present the first coupled cluster study of all three pyrrolyl isomers with a focus on providing spectroscopic constants needed for supporting experimental spectroscopy in the infrared and microwave regions. For each isomer we compute equilibrium geometries, harmonic and anharmonic vibrational frequencies and intensities, equilibrium and ground-state rotational constants, dipole moment projections, and spin-rotation and hyperfine coupling parameters. These are, to the best of our knowledge, the first reported vibrational frequencies for 2- and 3-pyrrolyl, as well as the first complete set of rotational spectroscopic parameters for any of the three isomers. Where data are available, we compare the results of our calculations with earlier experimental and theoretical calculations. Prospects for the spectroscopic detection of these radicals in different spectral regions are discussed. It is hoped that the results presented here will enable new experimental studies of pyrrolyl kinetics and dynamics and potentially enable its detection in astrophysical environments.

Methods

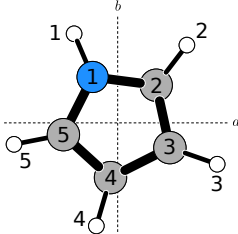
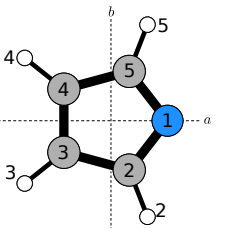
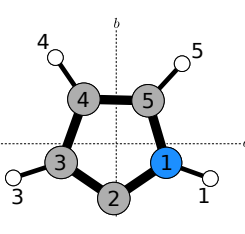
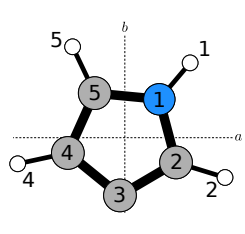
Calculations were performed with the CFOUR quantum chemistry package.⁴⁵ Unless indicated otherwise, all calculations were performed using an Unrestricted Hartree-Fock (UHF) reference. Structures previously calculated at the (U)B3LYP/cc-pVTZ⁴⁴ level were optimized with the coupled cluster method⁴⁶ with iterative inclusion of single and double excitations and up to perturbative inclusion of triple excitations [CCSD(T)]⁴⁷ and the Dunning polarized weighted core-valence basis sets (cc-pwCVXZ).⁴⁸ Initial geometry optimizations were done at the ae-CCSD/cc-pwCVDZ level of theory (all electrons correlated), followed by ae-CCSD(T)/cc-pwCVDZ, and finally at ae-CCSD(T)/cc-pwCVTZ.

To evaluate vibrational terms, the quadratic, cubic, and partial quartic force constants were evaluated via finite differences of analytic gradients under the frozen-core (fc) approximation. Restricted open-shell Hartree-Fock (ROHF) was used as a reference for 1-pyrrolyl. These calculations were performed at fc-CCSD(T) with the Ames Atomic Natural Orbital basis ANO0⁴⁹ from a reference geometry optimized using the same level of theory. The force constants and displacements were used to evaluate the harmonic vibrational frequencies and intensities, centrifugal distortion coefficients, and vibration-rotation interaction terms, and anharmonic vibrational frequencies were evaluated using second-order vibrational perturbation theory (VPT2).⁵⁰

Electronic spin-rotation tensors⁵¹ were calculated at the final optimized geometry using multiple levels of theory: selected combinations of fc-CCSD, ae-CCSD, ae-CCSD(T) with ANO0 as well as the Dunning cc-pVXZ ($X = D, T$),⁵² cc-pwCVXZ ($X = D, T$), and aug-cc-pVDZ⁵³ basis sets. Electric dipole moments, nitrogen quadrupole tensors, spin-spin coupling tensors, and Fermi contact terms were calculated at ae-CCSD(T)/cc-pwCVTZ.

Additional discussion of the choice of methods is provided in the next section.

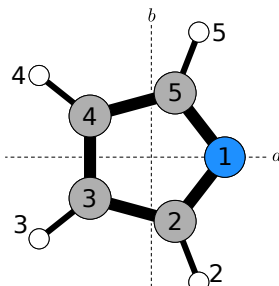
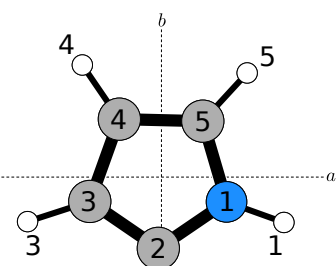
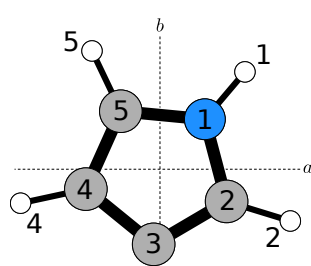
Table 1: Equilibrium geometries (in Angstrom and degrees) and relative energies^a (in kJ/mol) calculated at CCSD(T)/cc-pwCVTZ.

| | Pyrrole ^b | 1-Pyrrolyl | 2-Pyrrolyl | 3-Pyrrolyl |
|-----------|---|---|--|---|
| |  |  |  |  |
| N1-C2 | 1.370 | 1.345 | 1.356 | 1.379 |
| C2-C3 | 1.382 | 1.458 | 1.363 | 1.364 |
| C3-C4 | 1.417 | 1.360 | 1.436 | 1.412 |
| C4-C5 | 1.382 | 1.458 | 1.371 | 1.379 |
| C5-N1 | 1.370 | 1.345 | 1.382 | 1.368 |
| N1-H1 | 0.996 | – | 1.001 | 1.003 |
| C2-H2 | 1.076 | 1.080 | – | 1.074 |
| C3-H3 | 1.077 | 1.077 | 1.074 | – |
| C4-H4 | 1.077 | 1.077 | 1.077 | 1.075 |
| C5-H5 | 1.076 | 1.080 | 1.076 | 1.076 |
| ∠C2-N1-C5 | 109.8 | 104.4 | 107.9 | 110.1 |
| ∠N1-C2-C3 | 107.7 | 112.6 | 111.3 | 105.5 |
| ∠N1-C5-C4 | 107.7 | 112.6 | 107.8 | 108.7 |
| ∠C2-C3-C4 | 107.9 | 105.2 | 104.6 | 110.8 |
| ∠C5-C4-C3 | 107.9 | 105.2 | 108.4 | 104.9 |
| ∠C2-N1-H1 | 125.1 | – | 126.0 | 125.0 |
| ∠N1-C2-H2 | 121.5 | 120.9 | – | 122.0 |
| ∠N1-C5-H5 | 121.5 | 120.9 | 121.0 | 121.0 |
| ∠C2-C3-H3 | 127.1 | 126.3 | 127.7 | – |
| ∠C5-C4-H4 | 127.1 | 126.3 | 125.7 | 126.4 |
| | | Rel. Energy 0.00 | Rel. Energy +106.35 | Rel. Energy +105.08 |

^aRelative energies include anharmonic zero-point vibrational energies calculated at fc-CCSD(T)/ANO0.

^bExperimental values measured by Nygaard et al.⁵⁴ Uncertainties are ± 0.005 Å for bond length measurements and $\pm 0.5^\circ$ for bond angles.

Table 2: Mulliken analysis of ae-CCSD(T)/cc-pwCVTZ spin densities.

| | 1-Pyrrolyl | | 2-Pyrrolyl | | 3-Pyrrolyl | |
|------|---|----------------------|--|----------------------|---|----------------------|
| |  | |  | |  | |
| Atom | This Work | Ref. 22 ^a | This Work | Ref. 22 ^a | This Work | Ref. 22 ^a |
| N1 | -0.14 | -0.13 | -0.02 | -0.01 | 0.01 | -0.02 |
| C2 | 0.52 | 0.48 | 0.95 | 1.02 | -0.02 | -0.08 |
| C3 | 0.08 | 0.09 | 0.00 | -0.09 | 0.96 | 1.08 |
| C4 | 0.08 | 0.09 | 0.00 | 0.05 | 0.02 | -0.09 |
| C5 | 0.52 | 0.48 | 0.05 | 0.02 | -0.01 | 0.04 |
| H1 | - | | 0.00 | | 0.01 | |
| H2 | -0.03 | | - | | 0.00 | |
| H3 | -0.01 | | 0.00 | | - | |
| H4 | -0.01 | | 0.01 | | 0.00 | |
| H5 | -0.03 | | 0.00 | | 0.01 | |

^a Calculated at ω B97X-V/cc-pVTZ.

Results & Discussion

Energies and Geometries

The Born-Oppenheimer equilibrium structures and electronic energies of 1-, 2-, and 3-pyrrolyl calculated at the ae-CCSD(T)/cc-pwCVTZ level are shown in Table 1, along with the experimentally derived structure of pyrrole for comparison.⁵⁴ Previous ae-CCSD(T) calculations with a core-valence basis set (cc-pCV n Z) for treating core correlation have been shown to provide accurate molecular properties and spectroscopic constants for the phenyl radical.⁵⁵ A benchmarking study of the cc-pCVXZ and cc-pwCVXZ basis sets demonstrated that cc-pwCVXZ shows a better convergence rate for molecular properties, notably equilibrium bond length, with increasing X,⁴⁸ and so the weighted core-valence basis sets were used in the present calculations.

Pyrrole is an aromatic molecule with 6 π electrons delocalized among the C and N $2p_z$ orbitals. In the ground 2A_2 state of 1-pyrrolyl, the N–H bond from pyrrole is replaced by a lone electron pair, and the unpaired electron nominally resides in the N $2p_z$ orbital, leaving 5 delocalized π electrons. The coupled cluster wavefunction for 1-pyrrolyl is well-described as a doublet electronic state with minimal spin contamination ($\langle S^2 \rangle = 0.747$). The spin densities, shown in Table 2, show that the unpaired electron is delocalized significantly among the N and two adjacent C atoms, and to a lesser extent the remaining C atoms. Relative to pyrrole, the partial loss in aromaticity results in the lengthening of the (equivalent) C2-C3 and C4-C5 bonds from 1.382 Å to 1.458 Å and the shortening of the C3-C4 bond from 1.417 Å to 1.360 Å in 1-pyrrolyl. Similar trends were obtained from unrestricted DFT and QCISD calculations. For ω B97X-V/cc-pVTZ,²² bond lengths and angles agree within 0.006 Å and 0.2°; for (U)B3LYP/cc-pVTZ,⁴⁴ within 0.004 Å and 0.2°; for (U)M06-2X/cc-pVTZ,⁴⁴ within 0.008 Å and 0.2°; for QCISD/6-311G(d,p),⁵⁶ within 0.011 Å (bond angles were not provided). The spin densities match those calculated at ω B97X-V/cc-pVTZ²²

within a few hundredths at each atom. Despite the significant distortion of the ring structure, 1-pyrrolyl is nevertheless the most stable isomer.

2- and 3-pyrrolyl are nearly equal in energy; including the fc-CCSD(T)/ANO0 zero-point corrections, they lie 106.35 and 105.08 kJ/mol higher than 1-pyrrole, respectively. These are well matched with the relative energies provided in the literature, all of which are calculated with unrestricted DFT methods (108.32 and 106.48,²² 103.34 and 101.67,⁴⁴ and 91.63 and 89.96⁴⁴ kJ/mol). The $\langle S^2 \rangle$ values for both species are 0.746 at ae-CCSD(T)/cc-pwCVTZ. In both 2- and 3-pyrrolyl, the spin density calculations (Table 2) show that the unpaired electron remains localized to the respective C atom, suggesting these species are more reactive than 1-pyrrolyl. While the bond lengths of 2- and 3-pyrrolyl are not significantly different than those of pyrrole, the bond angles are widened around the radical centers from 107.7° to 111.3° for 2-pyrrolyl and from 107.4° to 110.75° for 3-pyrrolyl. The trend in 1-pyrrolyl is the opposite; relative to pyrrole the C-N-C bond angle is reduced from 109.8° to 104.39°.

Like 1-pyrrolyl, these trends agree well with those in the literature. For 2-pyrrolyl, the ω B97X-V/cc-pVTZ²² bond lengths and angles agree within 0.004 Å and 0.3°; for (U)B3LYP/cc-pVTZ,⁴⁴ within 0.003 Å and 0.1°; for (U)M06-2X/cc-pVTZ,⁴⁴ within 0.005 Å and 0.1°; for QCISD/6-311G(d,p),⁵⁶ within 0.008 Å. For 3-pyrrolyl, the ω B97X-V/cc-pVTZ²² bond lengths and angles agree within 0.006 Å and 0.2°; for (U)B3LYP/cc-pVTZ,⁴⁴ within 0.006 Å and 0.3°; for (U)M06-2X/cc-pVTZ,⁴⁴ within 0.008 Å and 0.9°; for QCISD/6-311G(d,p),⁵⁶ within 0.009 Å. The ae-CCSD(T)/cc-pwCVTZ spin densities of 2- and 3-pyrrolyl show more variation relative to the ω B97V/cc-pVTZ values;²² most notably that the spin density is less localized on the radical centers compared with the DFT values.

Vibrational Modes

The fc-CCSD(T)/ANO0 vibrational frequencies and intensities are shown in Table 3 for all isomers. Harmonic values and the VPT2 anharmonic values are shown. The combination

of frozen-core CCSD(T) calculations with the ANO family of basis sets has been shown to provide good estimates of properties that depend on force constants, including vibrational frequencies, rotational centrifugal distortion terms, and vibration-rotation interaction corrections to rotational constants, even for open-shell molecules.⁵⁷⁻⁶⁰ For 1-pyrrolyl, UHF instabilities at some displacements yielded nonphysical force constants, a known issue for some open-shell systems.⁶¹ For this reason a ROHF reference was used for this isomer. Similar behavior was not observed for 2- and 3-pyrrolyl, potentially due to their lower symmetry, and the UHF reference was used for these calculations.

Table 3: fc-CCSD(T)/ANO0 harmonic (ω) and anharmonic frequencies (ν), in cm^{-1} , and harmonic and anharmonic intensities (Int.), in km/mol .

| Mode ^a | 1-Pyrrolyl | | | | 2-Pyrrolyl | | | | 3-Pyrrolyl | | | | | | |
|-------------------|-------------------|----------|-------|--------|------------|-------------------|----------|--------|------------|-------|-------------------|----------|-------|--------|--------|
| | Mode ^b | ω | Int. | ν | Int. | Mode ^b | ω | Int. | ν | Int. | Mode ^b | ω | Int. | ν | Int. |
| 7 | ν_{11}, A_2 | 488.7 | 0.00 | 478.7 | 0.00 | ν_{21}, A'' | 325.8 | 45.85 | 362.7 | 43.85 | ν_{21}, A'' | 403.0 | 71.40 | 408.0 | 69.43 |
| 8 | ν_{21}, B_1 | 541.0 | 17.35 | 532.1 | 17.99 | ν_{20}, A'' | 499.3 | 13.03 | 492.1 | 15.37 | ν_{20}, A'' | 543.4 | 6.97 | 535.7 | 7.69 |
| 9 | ν_{18}, B_2 | 668.3 | 8.78 | 558.6 | 7.89 | ν_{19}, A'' | 610.6 | 0.76 | 600.9 | 1.02 | ν_{19}, A'' | 632.9 | 2.13 | 620.7 | 1.69 |
| 10 | ν_{20}, B_1 | 700.9 | 59.40 | 683.1 | 57.09 | ν_{18}, A'' | 695.7 | 55.35 | 691.0 | 58.72 | ν_{18}, A'' | 665.0 | 12.31 | 662.2 | 10.65 |
| 11 | ν_{10}, A_2 | 815.0 | 0.32 | 801.8 | 0.16 | ν_{17}, A'' | 750.0 | 72.00 | 738.0 | 59.94 | ν_{17}, A'' | 747.3 | 87.43 | 736.4 | 84.57 |
| 12 | ν_{19}, B_1 | 815.6 | 0.00 | 791.5 | 0.00 | ν_{16}, A'' | 842.0 | 0.07 | 829.4 | 0.05 | ν_{16}, A'' | 828.3 | 0.65 | 816.6 | 0.25 |
| 13 | ν_8, A_1 | 869.5 | 11.00 | 847.7 | 7.94 | ν_{15}, A' | 846.0 | 3.10 | 849.0 | 1.25 | ν_{15}, A' | 852.8 | 2.68 | 840.4 | 2.36 |
| 14 | ν_9, A_2 | 885.3 | 0.00 | 856.9 | 0.00 | ν_{14}, A' | 878.9 | 1.20 | 867.8 | 3.96 | ν_{14}, A' | 877.9 | 2.05 | 866.8 | 1.72 |
| 15 | ν_{17}, B_2 | 924.6 | 0.01 | 902.6 | 0.01 | ν_{13}, A' | 1020.7 | 16.30 | 1001.2 | 2.17 | ν_{13}, A' | 1032.5 | 34.02 | 1003.1 | 2.55 |
| 16 | ν_7, A_1 | 1039.1 | 0.05 | 1010.6 | 2.34 | ν_{12}, A' | 1060.2 | 18.87 | 1037.6 | 18.11 | ν_{12}, A' | 1065.8 | 14.23 | 1035.8 | 8.53 |
| 17 | ν_{16}, B_2 | 1069.4 | 2.17 | 957.0 | 3.12 | ν_{11}, A' | 1103.8 | 10.65 | 1081.9 | 6.03 | ν_{11}, A' | 1149.4 | 3.18 | 1111.3 | 325.11 |
| 18 | ν_6, A_1 | 1084.2 | 32.12 | 1066.0 | 49.78 | ν_{10}, A' | 1166.8 | 8.81 | 1143.5 | 7.51 | ν_{10}, A' | 1168.2 | 0.29 | 1143.4 | 0.09 |
| 19 | ν_5, A_1 | 1188.6 | 1.53 | 1133.6 | 4.20 | ν_9, A' | 1245.7 | 2.48 | 1216.5 | 2.78 | ν_9, A' | 1232.0 | 6.19 | 1211.9 | 33.27 |
| 20 | ν_{15}, B_2 | 1284.3 | 0.02 | 1250.9 | 2.27 | ν_8, A' | 1373.8 | 2.07 | 1342.9 | 1.39 | ν_8, A' | 1386.2 | 1.11 | 1355.3 | 0.21 |
| 21 | ν_{14}, B_2 | 1349.0 | 38.69 | 1309.4 | 19.24 | ν_7, A' | 1412.6 | 18.66 | 1364.3 | 16.50 | ν_7, A' | 1441.0 | 8.15 | 1393.2 | 9.53 |
| 22 | ν_4, A_1 | 1447.3 | 18.81 | 1426.8 | 2.39 | ν_6, A' | 1460.8 | 22.92 | 1428.8 | 16.08 | ν_6, A' | 1489.4 | 17.17 | 1446.7 | 14.78 |
| 23 | ν_3, A_1 | 1549.1 | 0.28 | 1478.8 | 0.08 | ν_5, A' | 1562.9 | 0.96 | 1529.1 | 0.50 | ν_5, A' | 1537.2 | 2.99 | 1505.5 | 1.91 |
| 24 | ν_{13}, B_2 | 3226.2 | 14.98 | 3086.7 | 3.23 | ν_4, A' | 3259.1 | 1.92 | 3123.0 | 2.48 | ν_4, A' | 3269.9 | 0.41 | 3133.5 | 0.94 |
| 25 | ν_2, A_1 | 3230.7 | 2.81 | 3094.2 | 3.49 | ν_3, A' | 3286.9 | 1.37 | 3151.3 | 2.67 | ν_3, A' | 3291.8 | 1.45 | 3155.6 | 2.38 |
| 26 | ν_{12}, B_2 | 3254.2 | 5.64 | 3113.1 | 0.85 | ν_2, A' | 3295.3 | 0.15 | 3159.6 | 0.29 | ν_2, A' | 3299.6 | 0.19 | 3163.7 | 0.19 |
| 27 | ν_1, A_1 | 3275.1 | 1.35 | 3139.3 | 2.36 | ν_1, A' | 3695.4 | 101.88 | 3522.2 | 79.13 | ν_1, A' | 3676.3 | 74.61 | 3504.6 | 57.14 |

^a Normal modes ordered by Hessian eigenvalue.

^b Normal modes as numbered in the Herzberg convention.

A comparison between the fc-CCSD(T)/ANO0 harmonic vibrational frequencies calculated in this work and those calculated previously for 1-pyrrolyl^{22,31,39,62} is shown in Table 4. Three experimental frequencies, measured with threshold photoelectron spectroscopy of the pyrrolide anion,⁴² are also included. 1-pyrrolyl has C_{2v} symmetry: the A_2 and B_1 modes correspond to in-plane bending motions but the A_2 modes are IR inactive. The A_1 modes

correspond to symmetric in-plane stretching and out-of-plane bending motions, while the B_2 modes are asymmetric in-plane stretching and out-of-plane bending motions. The four highest frequencies, all over 3000 cm^{-1} , are the C–H stretching modes.

Our harmonic frequencies agree most closely with those calculated at B3LYP/6-311G(d,p),^{31,62} giving a root mean square deviation (RMSD) of 17.7 cm^{-1} . The RMSD between the present values and those calculated at ω B97X-V/cc-pVTZ²² is 28.3 cm^{-1} , with the greatest discrepancies between the ν_9 A_2 and ν_{19} B_1 modes. The CASPT2/aug-cc-pVTZ+ frequencies³⁹ give a rather large RMSD of 90.2 cm^{-1} , which is expected given the lower-level treatment of electron correlation together with the state-averaged reference space employed in the calculation to treat electronically excited states.

A comprehensive literature search only turned up a single set of anharmonic frequencies calculated at B3LYP/6-311G(d,p) by Cronin et al.³¹ The fc-CCSD(T)/ANO0 anharmonic frequencies generally match these well, but the B_2 modes ν_9 and ν_{17} are notably different; the RMSD is 36.2 cm^{-1} with these modes included, but drops to 19.8 cm^{-1} when they are removed. These two modes also have the largest deviations between the calculated harmonic and anharmonic frequencies, so it is possible that effects of symmetry breaking are still giving anomalously large higher-order force constants for these motions. For the experimental frequencies,⁴² our calculated anharmonic values are lower, especially for the ν_8 mode measured at $925 \pm 65\text{ cm}^{-1}$. The experimental bands were assigned on the basis of B3LYP/6-311++G(d,p) harmonic frequencies and Franck-Condon simulations from the pyrrolide anion to the 1-pyrrolyl radical. Further calculations involving vibronic coupling may shed more light on the nature of the experimental spectrum.

To the best of our knowledge, no vibrational frequencies have been previously reported for 2- or 3-pyrrolyl, both of which have C_s symmetry. The six lowest frequencies are all A'' out-of-plane bending modes, and all other modes are A' in-plane bending and stretching modes. Both isomers show a bright N–H stretching mode near 3500 cm^{-1} as well as three

Table 4: Comparison of fc-CCSD(T)/ANO0 1-pyrrolyl harmonic and anharmonic frequencies with literature values, in cm^{-1} .

| Mode | Harmonic | | | | | Anharmonic | | Experimental |
|-----------------|-----------|----------------------|----------------------|----------------------|----------------------|------------|----------------------|----------------------|
| | This work | Ref. 31 ^a | Ref. 62 ^b | Ref. 22 ^c | Ref. 39 ^d | This Work | Ref. 31 ^a | Ref. 42 ^e |
| ν_1, A_1 | 3275.1 | 3245.8 | 3245.7 | 3270.28 | 3396 | 3139.3 | 3118.4 | – |
| ν_2, A_1 | 3230.7 | 3198.1 | 3198.0 | 3220.19 | 3369 | 3094.2 | 3056.5 | – |
| ν_3, A_1 | 1549.1 | 1560.5 | 1560.7 | 1595.90 | 1655 | 1478.8 | 1486.3 | – |
| ν_4, A_1 | 1447.3 | 1434.1 | 1434.2 | 1474.31 | 1558 | 1426.8 | 1414.8 | 1464(20) |
| ν_5, A_1 | 1188.6 | 1204.4 | 1204.3 | 1222.06 | 1268 | 1133.6 | 1140.8 | – |
| ν_6, A_1 | 1084.2 | 1091.3 | 1091.4 | 1106.20 | 1163 | 1066.0 | 1061.9 | – |
| ν_7, A_1 | 1039.1 | 1042.7 | 1043.0 | 1056.39 | 1106 | 1010.6 | 1012.2 | 1012(25) |
| ν_8, A_1 | 869.5 | 883.0 | 883.1 | 887.04 | 932 | 847.7 | 857.4 | 925(65) |
| ν_9, A_2 | 885.3 | 912.8 | 913.1 | 946.32 | 932 | 856.9 | 896.9 | – |
| ν_{10}, A_2 | 815.0 | 823.3 | 823.5 | 853.67 | 861 | 801.8 | 800.1 | – |
| ν_{11}, A_2 | 488.7 | 491.9 | 492.1 | 504.23 | 533 | 478.7 | 485.4 | – |
| ν_{12}, B_2 | 3254.2 | 3226.0 | 3225.8 | 3249.43 | 3376 | 3113.1 | 3096.3 | – |
| ν_{13}, B_2 | 3226.2 | 3193.9 | 3193.8 | 3215.39 | 3362 | 3086.7 | 3051.4 | – |
| ν_{14}, B_2 | 1349.0 | 1355.8 | 1355.8 | 1379.09 | 1474 | 1309.4 | 1329.6 | – |
| ν_{15}, B_2 | 1284.3 | 1291.6 | 1291.8 | 1303.57 | 1408 | 1250.9 | 1260.7 | – |
| ν_{16}, B_2 | 1069.4 | 1075.9 | 1075.3 | 1092.51 | 1156 | 957.9 | 1052.7 | – |
| ν_{17}, B_2 | 924.6 | 933.6 | 934.0 | 954.05 | 997 | 902.6 | 920.3 | – |
| ν_{18}, B_2 | 668.3 | 656.1 | 655.6 | 669.03 | 710 | 558.6 | 664.1 | – |
| ν_{19}, B_1 | 815.6 | 839.6 | 840.0 | 865.44 | 867 | 791.5 | 821.9 | – |
| ν_{20}, B_1 | 700.9 | 714.8 | 714.6 | 728.16 | 757 | 683.1 | 700.3 | – |
| ν_{21}, B_1 | 541.0 | 544.2 | 544.3 | 548.04 | 586 | 532.1 | 534.0 | – |

^{a,b} B3LYP/6-311G(d,p).

^c ω B97X-V/cc-pVTZ. Mode labels are estimated from frequencies and intensities.

^d SA-CASSCF(8,7)/CASPT2/aug-cc-pVTZ+.

^e Threshold photoelectron spectroscopy.

C–H stretching modes around 3150 cm^{-1} . In addition, the ν_{21} mode shows a negative anharmonicity in both isomers, and this mode participates in several combination band transitions as discussed more below. Of particular note, the 3-pyrrolyl ν_{11} mode in Table 3 shows a suspiciously large anharmonic intensity contribution, which should be viewed with caution.

Rotational Constants and Vibration-Rotation Interaction

The equilibrium rotational constants, vibration-rotation corrections, and centrifugal distortion constants in Watson’s A -reduction⁶³ are shown in Table 5, along with the projections of the dipole moment along the principal axes. The magnitudes of the vibration-rotation corrections are $\sim 1\%$ or less in all cases, and no individual vibration-rotation interaction constant for any mode or axis exceeds 60 MHz. After inclusion of these corrections, the inertial defects are all very small in magnitude (0.063, -0.003 , and 0.014 amu \AA^2), giving confidence in the reliability of the vibration-rotation terms.

All pyrrolyl isomers have a stronger total dipole moment than pyrrole (1.74 D^{54}), making them good candidates for rotational spectroscopy. By symmetry, 1-pyrrolyl has only a -type rotational transitions ($\mu_a = 2.02\text{ D}$), while 2- and 3-pyrrolyl have both a - and b -type transitions. The b -type transitions in 2-pyrrolyl are predicted to be significantly weaker than the a -type, as $\mu_a = 1.78\text{ D}$ while $\mu_b = 0.22\text{ D}$. In 3-pyrrolyl, the b -type transitions are predicted to be the strongest, with $\mu_b = 2.29\text{ D}$ and $\mu_a = 1.22\text{ D}$.

Electronic Spin-Rotation Coupling

For open-shell molecules, coupling between the electronic spin angular momentum and the rotational angular momentum leads to splittings of the rotational energy levels. Electronic spin-rotation coupling terms have not previously been calculated for any of the pyrrolyl isomers. Table 6 shows the diagonal elements of spin-rotation tensor for each isomer at

the ae-CCSD(T)/ANO0 level of theory. Complete spin-rotation tensors computed with a variety of methods and basis sets are reported in the Supplemental Information. The ae-CCSD(T)/ANO0 method has been shown to accurately predict experimentally-measured spin-rotation coefficients for 2-furanyloxy, another open-shell 5-member heterocycle.⁵⁹ However, it has been shown that spin-rotation tensor calculations at the same level of theory on different molecules do not necessarily result in the same degree of accuracy.⁵¹ Our additional calculations all give consistent values for the tensor elements.

Table 5: ae-CCSD(T)/cc-pwCVTZ equilibrium rotational constants of 1-, 2-, and 3-pyrrolyl with fc-CCSD(T)/ANO0 vibration-rotation and centrifugal distortion terms, in MHz unless otherwise noted.

| Parameter | 1- | 2- | 3- |
|------------------------------------|----------|----------|----------|
| A_e | 10020.21 | 10289.08 | 10307.28 |
| B_e | 8821.32 | 8935.88 | 8990.49 |
| C_e | 4691.31 | 4782.43 | 4801.98 |
| $A_e - A_0^a$ | 103.86 | 82.09 | 71.24 |
| $B_e - B_0^a$ | 38.89 | 64.37 | 71.45 |
| $C_e - C_0^a$ | 36.51 | 36.02 | 36.47 |
| $10^3 \Delta_N^a$ | 1.67 | 1.44 | 1.53 |
| $10^3 \Delta_{NK}^a$ | 2.93 | 0.57 | 0.07 |
| $10^3 \Delta_K^a$ | -1.39 | 2.12 | 2.52 |
| $10^4 \delta_N^a$ | 6.64 | 5.56 | 5.99 |
| $10^3 \delta_K^a$ | 3.08 | 1.54 | 1.42 |
| μ_a (D) | 2.02 | 1.78 | 1.22 |
| μ_b (D) | - | 0.22 | 2.29 |
| Δ_e^b (amu \AA^2) | 0.000 | 0.000 | 0.000 |
| Δ_0^b (amu \AA^2) | 0.063 | -0.003 | 0.014 |

^a Calculated at fc-CCSD(T)/ANO0.

^b Inertial defect: $I_c - I_a - I_b$.

The diagonal tensor elements are quite similar for 2- and 3-pyrrolyl; the ϵ_{aa} term is nearly an order of magnitude larger than ϵ_{bb} and ϵ_{cc} , which are within ~ 1 MHz of each other in magnitude but are opposite in sign, with a negative ϵ_{cc} value. For the 1-pyrrolyl isomer, ϵ_{aa} is the largest in magnitude and negative, ϵ_{cc} is one order of magnitude smaller and is

Table 6: CCSD(T)/cc-pwCVTZ ground-state rotational constants and hyperfine parameters for 1-, 2-, and 3- pyrrolyl, in MHz.

| Parameter ^a | 1- | 2- | 3- |
|------------------------|------------------------------|----------|----------|
| A_0^b | 9916.35 | 10207.00 | 10236.04 |
| B_0^b | 8782.43 | 8871.51 | 8919.04 |
| C_0^b | 4654.80 | 4746.41 | 4765.51 |
| ϵ_{aa}^c | -9.31 | 16.96 | 9.56 |
| ϵ_{bb}^c | 0.10 | 3.85 | 3.16 |
| ϵ_{cc}^c | -1.05 | -2.71 | -3.37 |
| χ_{aa} | -4.05 | 1.47 | 1.35 |
| χ_{bb} | 1.78 | 1.58 | 1.56 |
| χ_{cc} | 2.28 | -3.05 | -2.91 |
| $a_F(\text{N})$ | -8.24 (-8.16) ^d | 16.05 | 23.60 |
| $T_{aa}(\text{N})$ | 4.01 | 1.11 | -0.59 |
| $T_{bb}(\text{N})$ | 4.04 | 2.40 | 2.96 |
| $T_{cc}(\text{N})$ | -8.05 | -3.51 | -2.37 |
| $a_F(\text{H1})$ | - | 12.92 | 14.93 |
| $T_{aa}(\text{H1})$ | - | 12.67 | 0.50 |
| $T_{bb}(\text{H1})$ | - | -4.95 | 2.88 |
| $T_{cc}(\text{H1})$ | - | -7.71 | -3.38 |
| $a_F(\text{H2})$ | -36.20 (-37.18) ^d | - | 6.96 |
| $T_{aa}(\text{H2})$ | -14.31 | - | 9.69 |
| $T_{bb}(\text{H2})$ | 14.45 | - | -3.87 |
| $T_{cc}(\text{H2})$ | -0.14 | - | -5.82 |
| $a_F(\text{H3})$ | -9.10 (-9.95) ^d | 8.24 | - |
| $T_{aa}(\text{H3})$ | 6.61 | 11.32 | - |
| $T_{bb}(\text{H3})$ | -4.13 | -4.25 | - |
| $T_{cc}(\text{H3})$ | -2.49 | -7.07 | - |
| $a_F(\text{H4})$ | -9.10 (-9.95) ^d | 18.91 | 10.82 |
| $T_{aa}(\text{H4})$ | 6.61 | 0.63 | 10.53 |
| $T_{bb}(\text{H4})$ | -4.13 | 2.64 | -4.43 |
| $T_{cc}(\text{H4})$ | -2.49 | -3.27 | -6.10 |
| $a_F(\text{H5})$ | -36.20 (-37.18) ^d | 6.04 | 18.14 |
| $T_{aa}(\text{H5})$ | -14.31 | 0.31 | 0.28 |
| $T_{bb}(\text{H5})$ | 14.45 | 3.01 | 2.84 |
| $T_{cc}(\text{H5})$ | -0.14 | -3.33 | -3.12 |

^a Hydrogen labels match those in Tables 1 and 2. ^b Calculated from parameters in Table 5, $A_e - (A_e - A_0)$. ^c Calculated at ae-CCSD(T)/ANO0. ^d Measured with electron spin resonance spectroscopy⁴³ with uncertainty of ± 0.085 MHz.

also negative, and ϵ_{bb} is an order of magnitude smaller still and is positive. These trends arise because the natures of the electronic wavefunctions are similar as discussed previously: 2- and 3-pyrrolyl are both σ -type radicals while 1-pyrrolyl is better described as a π -type radical. The remaining differences are primarily associated with the different orientations of the principal axes. For 2- and 3- pyrrolyl, the spin density is oriented along the b molecular axis, while for 1-pyrrolyl it is more delocalized.

Table 7: Calculated Fermi contact coupling constants for carbon-13, in MHz.

| Parameter ^a | 1- | 2- | 3- |
|------------------------|--------|--------|--------|
| $a_F(\text{C2})$ | 34.14 | 506.76 | 69.30 |
| $a_F(\text{C3})$ | – | 43.00 | 39.65 |
| $a_F(\text{C4})$ | –10.56 | 50.93 | 460.05 |
| $a_F(\text{C5})$ | – | 39.33 | 37.92 |

^aAtom labels match those in Tables 1 and 2.

Hyperfine Interactions and Nuclear Spin Statistics

In addition to the electronic spin-rotation interaction, several other sources of angular momentum in the pyrrolyl radical split the rotational energy levels. The spin-1 ^{14}N nucleus has coupling of its electric quadrupole moment with the electric field gradient at the nucleus as well as dipolar electron spin-nuclear spin coupling. Spin-spin coupling also arises from the spin-1/2 H nuclei, which possess magnetic moments. Additionally, each $I > 0$ nucleus has a Fermi contact interaction arising from spin density within the volume of the nucleus. All of these coupling terms have been calculated at the ae-CCSD(T)/cc-pwCVTZ for each pyrrolyl isomer. The Fermi contact a_F terms, the diagonal elements of the nitrogen quadrupole coupling tensor (χ_{aa} , etc.), and the diagonal elements of the dipolar spin-spin coupling tensors (T_{aa} , etc.) are listed in Table 6. Complete tensors are provided in the Supplemental Information.

The ^{14}N -quadrupole coupling tensors follow a similar trend to the electron spin-rotation

coupling tensors. The diagonal elements of the 2- and 3-pyrrolyl χ tensors are quite similar to those for pyrrole (in MHz, $\chi_{aa} = 1.40475(181)$, $\chi_{bb} = 1.29577(203)$, $\chi_{cc} = -2.70052(272)$),⁶⁴ while those of 1-pyrrolyl resemble those of pyridine (in MHz, $\chi_{aa} = -4.91224(147)$, $\chi_{bb} = 1.43083(151)$, $\chi_{cc} = -3.48141(211)$).⁶⁴ This suggests that the electronic structure local to the nitrogen is not much altered by the dissociation of either C–H bond, as the unpaired electron remains localized to the respective carbon in 2- and 3-pyrrolyl. The electronic environment near the nitrogen in 1-pyrrolyl, however, is more consistent with a π -aromatic system combined with a lone pair in a σ -type molecular orbital in the molecular plane.

The electronic structure trends are also reflected in the Fermi contact terms, particularly those for ^{13}C shown in Table 7. The magnitudes of the Fermi contact terms are proportional to the spin density at the nuclear center: positive terms correspond to excess α density and negative terms to excess β density. In 1-pyrrolyl, all values are either negative or weakly positive because the unpaired electron is primarily delocalized among π orbitals above and below the nuclear plane. Meanwhile, 2- and 3-pyrrolyl have large positive values on the radical center where the unpaired electron lies in a σ -type orbital and weakly positive values elsewhere.

Finally, 1-pyrrolyl has two sets of equivalent hydrogen atoms, and therefore rotational transition intensities are affected by nuclear spin statistics. In C_{2v} , the nuclear spin wavefunction symmetry is $10A_1 \oplus 6B_1$, the former of which combine with even K_a rotational wavefunctions and the latter combine with odd K_a wavefunctions owing to the A_2 symmetry of the ground electronic state.^{65,66} As a result, there is a 5:3 ratio of statistical weights for the even:odd K_a rotational energy levels.

Implications for Laboratory Spectroscopy and Astronomy

Vibrational, Rovibrational, and Vibronic Spectroscopy

To date, three vibrational transitions have been measured and assigned to 1-pyrrolyl using threshold photoelectron spectroscopy.⁴² No experimental measurements have been reported for 2- or 3-pyrrolyl, and prior to this work, no theoretical predictions of harmonic frequencies were available. Since the photoelectron measurements in 2004, developments in vibrational spectroscopy make the pyrrolyl radicals attractive targets. Vibrational transitions of the pyridyl radical have been recently measured by cryogenically cooled slow photoelectron velocity map imaging (cryo-SEVI)⁶⁷ and matrix isolation infrared spectroscopy.⁶⁸ Stable 5-membered heterocycles have been studied with rotational resolution using Fourier transform infrared spectroscopy with synchrotron sources (e.g., including pyrrole,⁶⁹ furan,⁷⁰ thiophene⁷¹), and with an appropriate plasma source or F-abstraction technique,⁷² the pyrrolyl radicals may be amenable to detection using these methods.

Simulated anharmonic spectra for the pyrrolyl radicals, evaluated using *fc*-CCSD(T)/ANO0 force constants with VPT2, are shown in Figure 1. A complete list of the transition frequencies and intensities for the non-fundamental modes are provided in the Supporting Information. No additional treatments of Fermi or Coriolis resonances have been performed. For 1-pyrrolyl, the strongest transition is, surprisingly, calculated to be the $2\nu_{21}$ overtone at 1054 cm^{-1} . As this involves an out-of-plane bending vibrational mode, symmetry-breaking effects may induce significant changes in the electronic wavefunction at displaced geometries even without a noticeable error in energy,⁶¹ so this intensity should be viewed with caution. Other bright modes include the ν_{20} fundamental transition at 683 cm^{-1} and the ν_6 fundamental at 1066 cm^{-1} . The C–H stretching modes near 3100 cm^{-1} are comparable in intensity to several combination band transitions: $\nu_{10} + \nu_{20}$ and $\nu_{16} + \nu_{18}$ at 1485 cm^{-1} ,

$\nu_3 + \nu_{18}$ at 1999 cm^{-1} and $\nu_4 + \nu_{18}$ at 2075 cm^{-1} . These combination band transitions are particularly attractive targets as they lie in a region free from any pyrrole transitions of significant intensity.⁷³

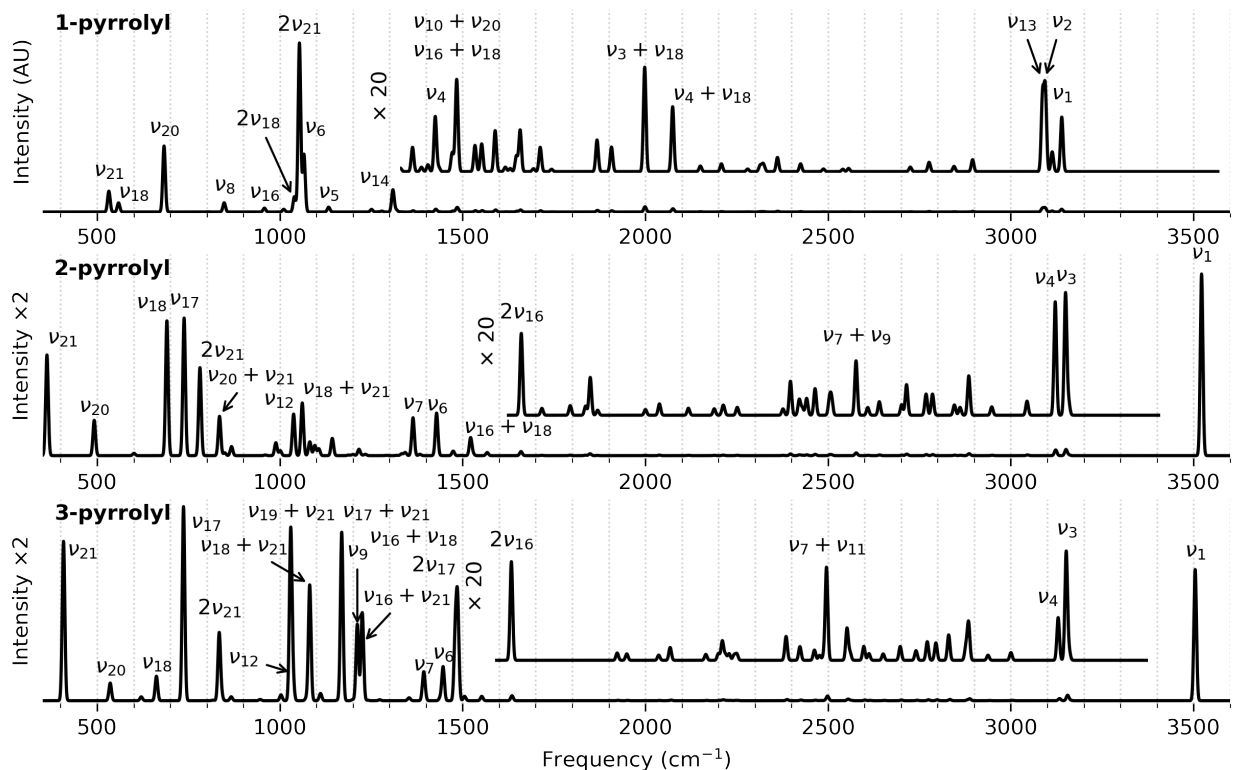


Figure 1: Simulated VPT2 anharmonic vibrational spectra of pyrrolyl radical isomers calculated at fc-CCSD(T)/ANO1 and convolved to a linewidth of 3 cm^{-1} . Insets show the spectrum magnified by a factor of 20. Labels indicate several of the strongest modes; a complete list of frequencies and intensities is provided in the Supporting Information. For 3-pyrrolyl, the intensity for the ν_{11} mode at 1100 cm^{-1} (not labeled) is plotted using the harmonic value; all other modes in all three plots use anharmonic intensities.

Spectra of 2- and 3-pyrrolyl can be readily distinguished by the presence of the bright N–H stretching mode (ν_1) near 3500 cm^{-1} , as well as three A'' modes below 900 cm^{-1} that correspond to IR-inactive A_2 modes in 1-pyrrolyl. The ν_1 mode of 3-pyrrolyl is calculated to lie 18 cm^{-1} below that of 2-pyrrolyl, which in turn is 8 cm^{-1} below the ν_1 mode of pyrrole.⁷³ Assuming both isomers are present in the same environment, the $700\text{--}1200\text{ cm}^{-1}$ region features several transitions that readily distinguish the two. In particular, two combination

bands involving ν_{21} near 1200 cm^{-1} ($\nu_{17} + \nu_{21}$ at 1169 cm^{-1} and $\nu_{16} + \nu_{21}$ at 1226 cm^{-1}) are especially bright in 3-pyrrole, while $\nu_{20} + \nu_{21}$ mode at 835 cm^{-1} is more distinct in 2-pyrrole.

A peak with $m/z = 66$, the nominal mass of $\text{C}_4\text{H}_4\text{N}$, was detected in Titan’s atmosphere by the Cassini ion-neutral mass spectrometer.¹⁷ Radicals are thought to play an important role in Titan’s atmospheric chemistry,²¹ and the cyclic reactive molecule cyclopropenylidene ($c\text{-C}_3\text{H}_2$) was recently detected at high altitudes with the Atacama Large Millimeter Array. Infrared observations with the James Webb Space Telescope (JWST) may provide a means for detecting additional reactive species. The mid infrared instrument aboard JWST will have its greatest signal-to-noise ratio and spectral resolution in the $800\text{--}2000\text{ cm}^{-1}$ range.⁷⁴ The large CH_4 concentration in Titan’s atmosphere will dominate the spectrum near 1300 cm^{-1} , but each pyrrolyl isomer has at least one bright mode in the $800\text{--}1200\text{ cm}^{-1}$ range that can be targeted. 3-pyrrolyl also has a strong overtone transition $2\nu_{17}$ at 1480 cm^{-1} and a combination band $\nu_{16} + \nu_{18}$ at 1486 cm^{-1} that may be observable.

Rotational Spectroscopy

Pure rotational spectroscopy has proven to be a powerful method for detecting transient molecular species, and the pyrrolyl radicals would appear to be excellent targets. Pulsed discharge nozzle expansions coupled with chirped-pulse and/or cavity Fourier transform microwave (FTMW) spectroscopy has led to the identification of a number of radicals in the $2\text{--}90\text{ GHz}$ range, including C_6H_5 ,⁷⁵ HOCO ,⁷⁶ and $\text{H}_2\text{C}_3\text{N}$ ⁶⁰ among many others. Pyrolysis nozzles are also used in conjunction with FTMW spectroscopy to effectively generate radicals such as $\text{C}_6\text{H}_5\text{O}$ ⁷⁷ and $\text{C}_4\text{H}_3\text{O}_2$.⁵⁹ In addition, the recent use of buffer gas cooling cells with chirped-pulse FTMW spectroscopy^{78,79} has enabled new high-sensitivity measurements owing to their large duty cycles, and addition of a pyrolysis or discharge source would make production of pyrrolyl from pyrrole a possibility in these instruments as well. Toward higher frequencies, long-pass millimeter-wave frequency modulation spectroscopy is routinely em-

ployed with discharge or F-abstraction cells similar to those used with synchrotron sources to detect radicals.^{55,80–82}

To guide potential searches using molecular beam or buffer gas methods, simulated 4 K rotational spectra in the centimeter band are shown for all three isomers in Figure 2. All isomers are asymmetric tops, with $\kappa \approx 0.6$ for 1-pyrrolyl and 0.5 for 2- and 3-pyrrolyl. Each features a prominent *a*-type progressions with a large harmonic defect owing to the significant asymmetry: though $B_0 + C_0$ is ~ 13.5 GHz for each, these progressions are spaced by ~ 10 GHz. Changes in the orientation of the principal axes relative to the ring structure cause each rotational constant to follow the trend (1-pyrrolyl) < (2-pyrrolyl) < (3-pyrrolyl), making isomer discrimination especially simple in the pure rotational spectrum. The spectrum of 3-pyrrolyl additionally contains *b*-type transitions of appreciable intensity. Analogous transitions are present in the spectrum of 2-pyrrolyl but are much weaker owing to its small μ_b value, and they are not apparent in Figure 2.

The low- N transitions of all three radicals show complex structure arising from spin-rotation and hyperfine splitting, as shown in Figure 3. As N increases, the structure associated with nuclear spin collapses. The majority of the intensity in the hyperfine structure associated with the fundamental *a*-type ($N_{K_a K_c} = 1_{01} - 0_{00}$) rotational transition spans 20–30 MHz for all three radicals, and that of the fundamental *b*-type ($1_{11} - 0_{00}$) transition for 2- and 3-pyrrolyl. The $9_{09} - 8_{08}$ *a*-type rotational transition, which is heavily mixed with $9_{19} - 8_{18}$ and the *b*-type transitions $9_{19} - 8_{08}$ and $9_{09} - 8_{18}$ (2- and 3-pyrrolyl only) shows a much more compact structure spanning only 1–2 MHz. For 2- and 3-pyrrolyl, the two prominent clusters of peaks have clearly resolved into a spin-rotation doublet typical of a radical with a doublet electronic state, as shown with lower resolution in Figure 4. Similar collapse is observed in higher- N *b*-type transitions like the $9_{46} - 8_{35}$ transition shown in Figure 3. The spin-rotation doublet is beginning to become resolved in 2-pyrrolyl, and becomes more apparent at still greater N . This limited structure within higher N transitions makes

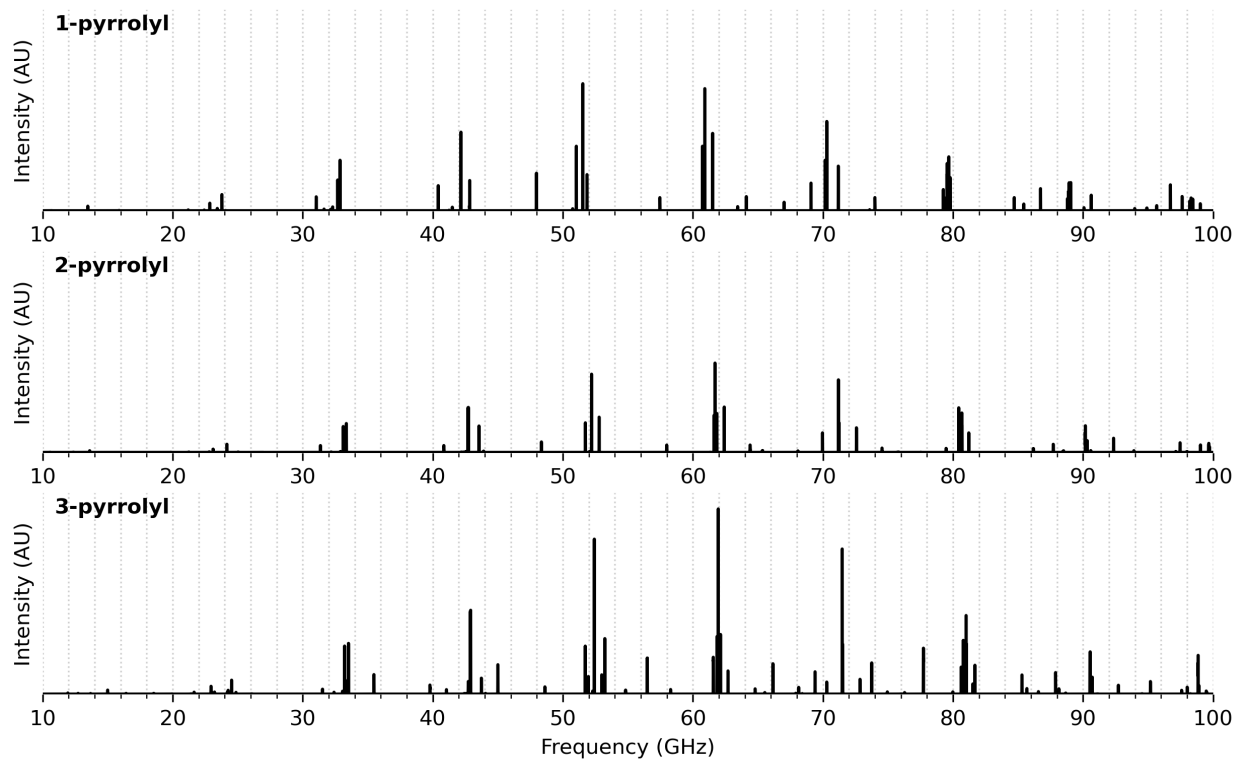


Figure 2: Simulated rotational spectra of pyrrolyl isomers in the 10–100 GHz frequency range at a temperature of 4 K. All panels use the same vertical scale for intensity comparisons. Rotational transitions are convolved to a linewidth of 3 MHz.

both spectroscopy and radio astronomy in the mm-wave region particularly promising; however, the transition frequencies predicted from the spectroscopic constants presented here are expected to be less accurate than those toward low frequencies.

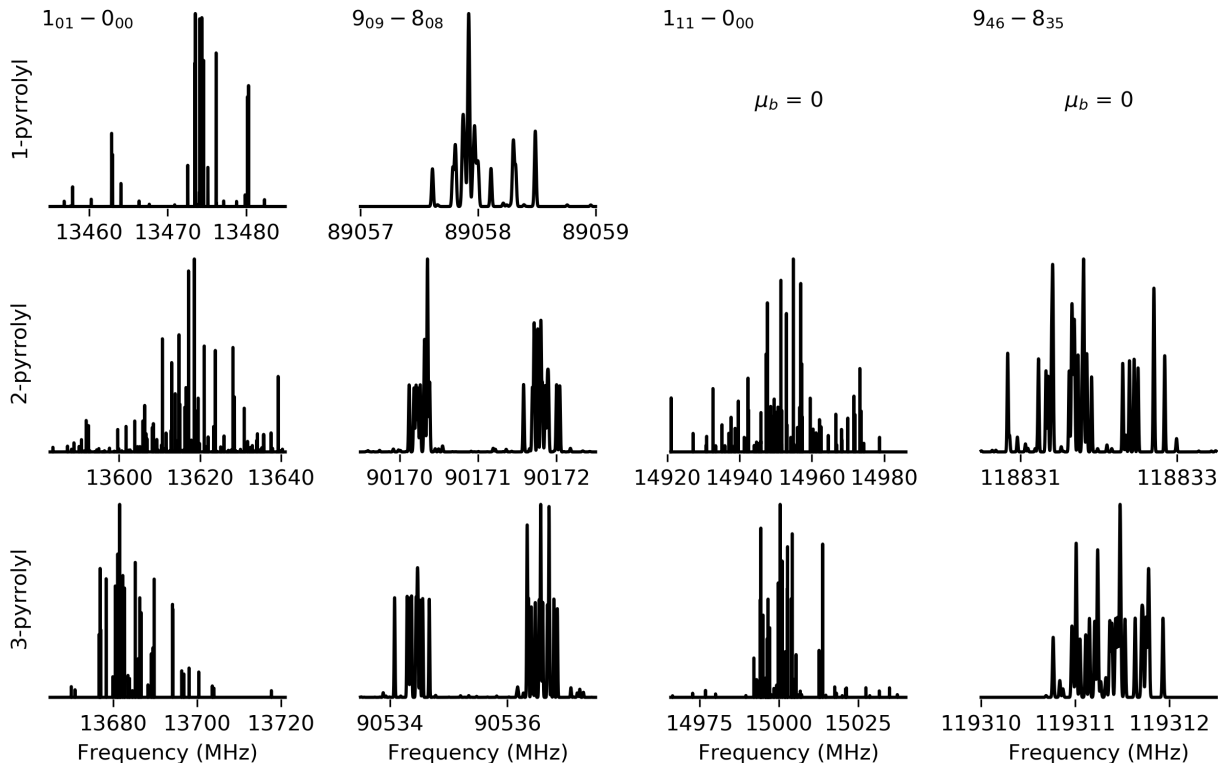


Figure 3: Simulated hyperfine splitting in selected a - and b -type rotational transitions of pyrrolyl radicals. Transitions are convolved to a linewidth of 10 kHz, and the vertical axis scale for each plot is different; relative intensities between plots are not to scale.

Conclusions

In this work, we have characterized the 1-, 2-, and 3-pyrrolyl radicals in their ground electronic states at the CCSD(T) level of theory with an emphasis on computing spectroscopic parameters for rotational and vibrational spectroscopy. Pyrrolyl radicals are important combustion intermediates and have been proposed to be able to form under the conditions of Titan’s atmosphere, but to date little spectroscopic information is available. Our CCSD(T)

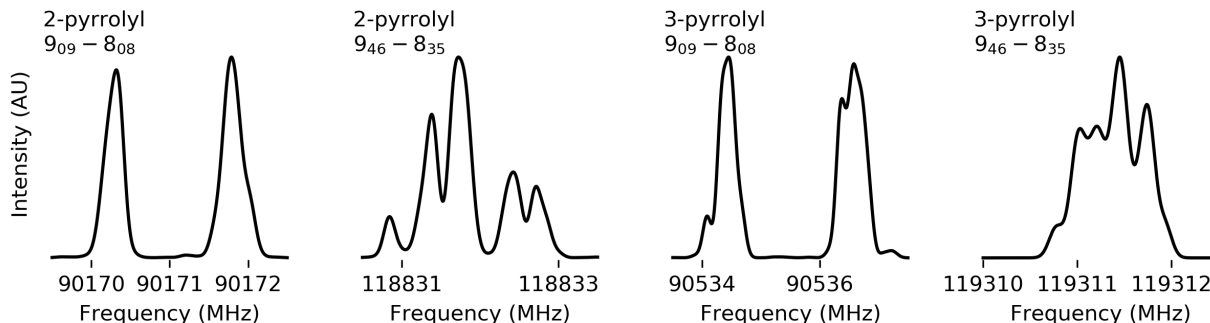


Figure 4: As Figure 3, but transitions are convolved to 100 kHz to show the collapse of hyperfine structure.

optimized equilibrium geometries, computed with full electron correlation, are in general agreement with previous DFT structures and obtain the same relative energy ordering: 1-pyrrolyl is the most stable, with 3-pyrrolyl lying 105 kJ/mol higher and 2-pyrrolyl 106 kJ/mol higher.

To evaluate parameters sensitive to the local potential energy surface, quadratic, cubic, and a subset of quartic force constants were derived from finite differences at displaced molecular geometries under the frozen core approximation at CCSD(T)/ANO0. These force constants were used to derive harmonic vibrational frequencies and intensities, vibration-rotation interaction coefficients, and centrifugal distortion constants. In addition, tensor elements were computed for the electron spin-rotation interaction, the dipolar electron spin-nuclear spin interactions for $I > 0$ nuclei, and the ^{14}N quadrupole interaction, as well as Fermi contact interactions for each $I > 0$ nucleus, which are in excellent agreement with isotropic coupling terms measured previously with electron spin resonance for 1-pyrrolyl.

Simulated anharmonic vibrational spectra were shown in Figure 1 in the 400–4000 cm^{-1} range covering all of the fundamental modes. In particular, several combination bands involving low-frequency bending modes for each isomer are calculated to carry significant intensity, providing distinctive infrared spectral signatures that distinguish each isomer from the others and from pyrrole. These isomers are amenable to detection by high-resolution

photoelectron methods such as cryo-SEVI or by matrix isolation infrared spectroscopy. The pure rotational spectra are simulated using ground-state rotational constants and all diagonal hyperfine tensor elements in Figures 2, 3, and 4. Each isomer has at least one dipole moment projection exceeding 1 D, and should be readily observable by FTMW methods if sufficient quantities of the radicals can be produced. At low frequencies, each rotational transition is split into many tens of lines due to angular momentum coupling, but most of this structure collapses by $N = 9$ near 100 GHz, so the prospects for detection in the millimeter-wave band (both in the laboratory and in space using ALMA) are promising, especially if initial observations in the centimeter band are made to refine the rotational constants.

Given their importance in N-containing pollution from biomass combustion, in situ spectroscopic measurements of the pyrrolyl radicals may yield fundamental mechanistic data needed help guide mitigation efforts. Laboratory spectroscopy is also a necessary precursor to astronomical observations seeking to identify these radicals in Titan’s atmosphere and in the interstellar medium. Our goal with this work is to enable these new laboratory spectroscopic investigations of the pyrrolyl radicals to be undertaken.

Acknowledgments

The authors thank John F. Stanton and K. L. Kelvin Lee for their invaluable help with the CFOUR calculations. The authors further thank Lee-Ping Wang and Kelly S. Meyer for useful discussions. S. L. J. was supported by NASA Headquarters under the NASA Earth and Space Science Fellowship Program- Grant 80NSSC18K1110.

Supporting Information

Anharmonic transitions and intensities (fc-CCSD(T)/ANO0, 1/2/3pyrr_anharm_transitions.txt), translational, rotational, and vibrational normal mode coordinates (fc-CCSD(T)/ANO0, 1/2/3pyrr_normal_mode_coords.txt), rotational constants for vibrationally excited states (fc-CCSD(T)/ANO0, 1/2/3pyrr_B_excited_vib_states.txt), full spin-rotation tensors at multiple levels of theory (supporting_info.pdf), ground state (vibrationally averaged) geometries (supporting_info.pdf), complete N quadrupole, N spin-spin, and H spin-spin hyperfine coupling terms with equilibrium geometries in Z-matrix (ae-CCSD(T)/cc-pwCVTZ, 1/2/3pyrr_full_rot_HF.txt).

References

- (1) Glarborg, P. Fuel nitrogen conversion in solid fuel fired systems. *Prog. Energy Combust. Sci.* **2003**, *29*, 89–113.
- (2) Sheng, L.; Wang, X.; Yang, X. Prediction model of biocrude yield and nitrogen heterocyclic compounds analysis by hydrothermal liquefaction of microalgae with model compounds. *Bioresour. Technol.* **2018**, *247*, 14–20.
- (3) Pershing, D. W.; Wendt, J. O. Relative contributions of volatile nitrogen and char nitrogen to NO_x emissions from pulverized coal flames. *Ind. Eng. Chem. Process. Des. Dev.* **1979**, *18*, 60–67.
- (4) Moller, L.; Lax, I.; Eriksson, L. C. Nitrated polycyclic aromatic hydrocarbons: A risk assessment for the urban citizen. *Environ. Health Perspect.* **1993**, *101*, 309–315.
- (5) Bünger, J.; Krahl, J.; Schröder, O.; Schmidt, L.; Westphal, G. A. Potential hazards

- associated with combustion of bio-derived versus petroleum-derived diesel fuel. *Crit. Rev. Toxicol.* **2012**, *42*, 732–750.
- (6) Oluwoye, I.; Altarawneh, M.; Gore, J.; Dlugogorski, B. Z. Products of incomplete combustion from biomass reburning. *Fuel* **2020**, *274*, 117805.
- (7) Martins, Z. The nitrogen heterocycle content of meteorites and their significance for the origin of life. *Life* **2018**, *8*, 28.
- (8) Kutner, M. L.; Machnik, D. E.; Tucker, K. D.; Dickman, R. L. Search for interstellar pyrrole and furan. *Astrophys. J.* **1980**, *242*, 541.
- (9) Myers, P. C.; Thaddeus, P.; Linke, R. A. A search for interstellar pyrrole - Evidence that rings are less abundant than chains. *Astrophys. J.* **1980**, *241*, 155.
- (10) McGuire, B. A. 2018 census of interstellar, circumstellar, extragalactic, protoplanetary disk, and exoplanetary molecules. *Astrophys. J., Suppl. Ser.* **2018**, *239*, 17.
- (11) Materese, C. K.; Nuevo, M.; Bera, P. P.; Lee, T. J.; Sandford, S. a. Thymine and other prebiotic molecules produced from the ultraviolet photo-irradiation of pyrimidine in simple astrophysical ice analogs. *Astrobiology* **2013**, *13*.
- (12) Materese, C. K.; Nuevo, M.; Sandford, S. A. N- and O-heterocycles produced from the irradiation of benzene and naphthalene in H₂O/NH₃-containing ices. *Astrophys. J.* **2015**, *800*, 116.
- (13) Nuevo, M.; Milam, S. N.; Sandford, S. A. Nucleobases and prebiotic molecules in organic residues produced from the ultraviolet photo-irradiation of pyrimidine in NH₃ and H₂O+NH₃ ices. *Astrobiology* **2012**, *12*, 295–314.
- (14) Öberg, K. I. Photochemistry and astrochemistry: Photochemical pathways to interstellar complex organic molecules. *Chem. Rev.* **2016**, *116*, 9631–9663.

- (15) Palmer, M. Y.; Cordiner, M. A.; Nixon, C. A.; Charnley, S. B.; Teanby, N. A.; Kisiel, Z.; Irwin, P. G. J.; Mumma, M. J. ALMA detection and astrobiological potential of vinyl cyanide on Titan. *Sci. Adv.* **2017**, *3*, e1700022.
- (16) Waite, J. H.; Niemann, H.; Yelle, R. V.; Kasprzak, W. T.; Cravens, T. E.; Luhmann, J. G.; McNutt, R. L.; Ip, W. H.; Gell, D.; De La Haye, V. et al. Ion Neutral Mass Spectrometer results from the first flyby of Titan. *Science* **2005**, *308*, 982–986.
- (17) Cravens, T. E.; Robertson, I. P.; Waite, J. H.; Yelle, R. V.; Kasprzak, W. T.; Keller, C. N.; Ledvina, S. A.; Niemann, H. B.; Luhmann, J. G.; McNutt, R. L. et al. Composition of Titan’s ionosphere. *Geophys. Res. Lett.* **2006**, *33*, L07105.
- (18) Vuitton, V.; Yelle, R.; McEwan, M. Ion chemistry and N-containing molecules in Titan’s upper atmosphere. *Icarus* **2007**, *191*, 722–742.
- (19) McGuire, B. A.; Burkhardt, A. M.; Kalenskii, S.; Shingledecker, C. N.; Remijan, A. J.; Herbst, E.; McCarthy, M. C. Detection of the aromatic molecule benzonitrile ($c\text{-C}_6\text{H}_5\text{CN}$) in the interstellar medium. *Science* **2018**, *359*, 202–205.
- (20) Cooke, I. R.; Gupta, D.; Messinger, J. P.; Sims, I. R. Benzonitrile as a proxy for benzene in the cold ISM: Low-temperature rate coefficients for $\text{CN} + \text{C}_6\text{H}_6$. *Astrophys. J.* **2020**, *891*, L41.
- (21) Krasnopolsky, V. A. A photochemical model of Titan’s atmosphere and ionosphere. *Icarus* **2009**, *201*, 226–256.
- (22) Hendrix, J.; Bera, P. P.; Lee, T. J.; Head-Gordon, M. Cation, anion, and radical isomers of $\text{C}_4\text{H}_4\text{N}$: Computational characterization and implications for astrophysical and planetary environments. *J. Phys. Chem. A* **2020**, *124*, 2001–2013.

- (23) Ikeda, E.; Nicholls, P.; Mackie, J. C. A kinetic study of the oxidation of pyridine. *Proc. Combust. Inst.* **2000**, *28*, 1709–1716.
- (24) Tian, Z.; Li, Y.; Zhang, T.; Zhu, A.; Cui, Z.; Qi, F. An experimental study of low-pressure premixed pyrrole/oxygen/argon flames with tunable synchrotron photoionization. *Combust. Flame* **2007**, *151*, 347–365.
- (25) Alzueta, M. U.; Tena, A.; Bilbao, R. Pyridine conversion in a flow reactor and its interaction with nitric oxide. *Combust. Sci. Technol.* **2002**, *174*, 151–169.
- (26) Lumberas, M.; Alzueta, M. U.; Bilbao, R. A study of pyrrole oxidation under flow reactor conditions. *Combust. Sci. Technol.* **2001**, *172*, 123–139.
- (27) Luo, J.; Zou, C.; He, Y.; Jing, H.; Cheng, S. The characteristics and mechanism of NO formation during pyridine oxidation in O₂/N₂ and O₂/CO₂ atmospheres. *Energy* **2019**, *187*, 115954.
- (28) Wu, L. N.; Tian, Z. Y.; Weng, J. J.; Yu, D.; Liu, Y. X.; Tian, D. X.; Cao, C. C.; Zou, J. B.; Zhang, Y.; Yang, J. Z. Experimental and kinetic study on the low-temperature oxidation of pyridine as a representative of fuel-N compounds. *Combust. Flame* **2019**, *202*, 394–404.
- (29) Yamamoto, T.; Kuwahara, T.; Nakaso, K.; Yamamoto, T. Kinetic study of fuel NO formation from pyrrole type nitrogen. *Fuel* **2012**, *93*, 213–220.
- (30) Blank, D. A.; North, S. W.; Lee, Y. T. The ultraviolet photodissociation dynamics of pyrrole. *Chem. Phys.* **1994**, *187*, 35–47.
- (31) Cronin, B.; Nix, M. G.; Qadiri, R. H.; Ashfold, M. N. High resolution photofragment translational spectroscopy studies of the near ultraviolet photolysis of pyrrole. *Phys. Chem. Chem. Phys.* **2004**, *6*, 5031–5041.

- (32) Lippert, H.; Ritze, H.-H.; Hertel, I. V.; Radloff, W. Femtosecond time-resolved hydrogen-atom elimination from photoexcited pyrrole molecules. *Chem. Phys. Chem.* **2004**, *5*, 1423–1427.
- (33) Roberts, G. M.; Williams, C. A.; Yu, H.; Chatterley, A. S.; Young, J. D.; Ullrich, S.; Stavros, V. G. Probing ultrafast dynamics in photoexcited pyrrole: Timescales for $^1\pi\sigma^*$ mediated H-atom elimination. *Faraday Discuss.* **2013**, *163*, 95.
- (34) Wei, J.; Kuczmann, A.; Riedel, J.; Renth, F.; Temps, F. Photofragment velocity map imaging of H atom elimination in the first excited state of pyrrole. *Phys. Chem. Chem. Phys.* **2003**, *5*, 315–320.
- (35) Rubio-Lago, L.; Zaouris, D.; Sakellariou, Y.; Sofikitis, D.; Kitsopoulos, T. N.; Wang, F.; Yang, X.; Cronin, B.; Devine, A. L.; King, G. A. et al. Photofragment slice imaging studies of pyrrole and the Xe-pyrrole cluster. *J. Chem. Phys.* **2007**, *127*, 064306.
- (36) Vallet, V.; Lan, Z.; Mahapatra, S.; Sobolewski, A. L.; Domcke, W. Photochemistry of pyrrole: Time-dependent quantum wave-packet description of the dynamics at the $^1\pi\sigma^*$ - S_0 conical intersections. *J. Chem. Phys.* **2005**, *123*, 144307.
- (37) Saita, K.; Nix, M. G. D.; Shalashilin, D. V. Simulation of ultrafast photodynamics of pyrrole with a multiconfigurational Ehrenfest method. *Phys. Chem. Chem. Phys.* **2013**, *15*, 16227.
- (38) Grebenschikov, S. Y.; Picconi, D. Fano resonances in the photoinduced H-atom elimination dynamics in the $\pi\sigma^*$ states of pyrrole. *Phys. Chem. Chem. Phys.* **2017**, *19*, 14902–14906.
- (39) Picconi, D.; Grebenschikov, S. Y. Photodissociation dynamics in the first absorption band of pyrrole. I. Molecular Hamiltonian and the Herzberg-Teller absorption spectrum for the $^1A_2(\pi\sigma^*) \leftarrow X^1A_1(\pi\pi)$ transition. *J. Chem. Phys.* **2018**, *148*, 104103.

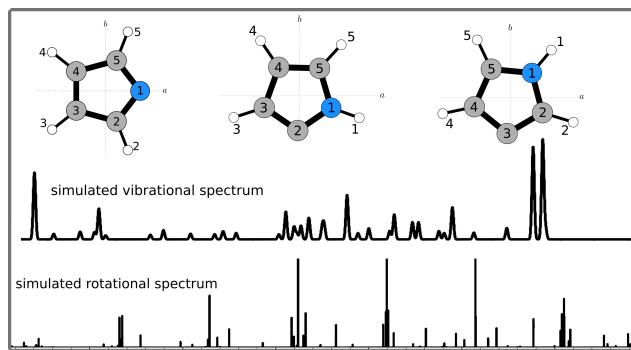
- (40) Nandipati, K. R.; Kanakati, A. K.; Singh, H.; Lan, Z.; Mahapatra, S. Initial state-specific photodissociation dynamics of pyrrole via $^1\pi\sigma^*/S_0$ conical intersection initiated with optimally controlled UV-laser pulses. *Eur. Phys. J. D* **2017**, *71*, 222.
- (41) Bacskay, G. B.; Martoprawiro, M.; Mackie, J. C. An ab initio quantum chemical study of the electronic structure and stability of the pyrrolyl radical: Comparison with the isoelectronic cyclopentadienyl radical. *Chem. Phys. Lett.* **1998**, *290*, 391–398.
- (42) Gianola, A. J.; Ichino, T.; Hoenigman, R. L.; Kato, S.; Bierbaum, V. M.; Carlisleberger, W. Thermochemistry and electronic structure of the pyrrolyl radical. *J. Phys. Chem. A* **2004**, *108*, 10326–10335.
- (43) Samuni, A.; Neta, P. Electron spin resonance study of the reaction of hydroxyl radicals with pyrrole, imidazole, and related compounds. *J. Phys. Chem* **1973**, *77*, 1629–1635.
- (44) Sah, C.; Kumar Yadav, A.; Venkataramani, S. Deciphering stability of five-membered heterocyclic radicals: Balancing Act Between Delocalization and Ring Strain. *J. Phys. Chem. A* **2018**,
- (45) Matthews, D. A.; Cheng, L.; Harding, M. E.; Lipparini, F.; Stopkowicz, S.; Jagau, T.-C.; Szalay, P. G.; Gauss, J.; Stanton, J. F. Coupled-cluster techniques for computational chemistry: The CFOUR program package. *J. Chem. Phys* **2020**, *152*, 214108.
- (46) Bartlett, R. J. Many-body perturbation theory and coupled cluster theory for electron correlation in molecules. *Annu. Rev. Phys. Chem.* **1981**, *32*, 359–401.
- (47) Raghavachari, K.; Trucks, G. W.; Pople, J. A.; Head-Gordon, M. A fifth-order perturbation comparison of electron correlation theories. *Chem. Phys. Lett.* **1989**, *157*, 479–483.

- (48) Peterson, K. A.; Dunning, T. H. Accurate correlation consistent basis sets for molecular core-valence correlation effects: The second row atoms Al-Ar, and the first row atoms B-Ne revisited. *J. Chem. Phys.* **2002**, *117*, 10548–10560.
- (49) Almlöf, J.; Taylor, P. R. General contraction of Gaussian basis sets. I. Atomic natural orbitals for first- and second-row atoms. *J. Chem. Phys.* **1987**, *86*, 4070–4077.
- (50) Mills, I. M. Vibration–rotation structure in asymmetric- and symmetric-top molecules. *Molecular Spectroscopy* **1972**, 115–140.
- (51) Tarczay, G.; Szalay, P. G.; Gauss, J. First-principles calculation of electron spin-rotation tensors. *J. Phys. Chem. A.* **2010**, *114*, 9246–9252.
- (52) Dunning, T. H. Gaussian basis sets for use in correlated molecular calculations. I. The atoms boron through neon and hydrogen. *J. Chem. Phys.* **1989**, *90*, 1007–1023.
- (53) Kendall, R. A.; Dunning, T. H.; Harrison, R. J. Electron affinities of the first-row atoms revisited. Systematic basis sets and wave functions. *J. Chem. Phys.* **1992**, *96*, 6796–6806.
- (54) Nygaard, L.; Nielsen, J. T.; Kirchheiner, J.; Maltesen, G.; Rastrup-Andersen, J.; Sørensen, G. O. Microwave spectra of isotopic pyrroles. Molecular structure, dipole moment, and ^{14}N quadrupole coupling constants of pyrrole. *J. Mol. Struct.* **1969**, *3*, 491–506.
- (55) Martinez, O.; Crabtree, K. N.; Gottlieb, C. A.; Stanton, J. F.; McCarthy, M. C. An accurate molecular structure of phenyl, the simplest aryl radical. *Angew. Chem.* **2015**, *54*, 1808–1811.
- (56) da Silva, G.; Moore, E. E.; Bozzelli, J. W. Quantum chemical study of the structure

- and thermochemistry of the five-membered nitrogen-containing heterocycles and their anions and radicals. *J. Phys. Chem. A* **2006**, *110*, 13979–13988.
- (57) Zhang, X.; Sander, S. P.; Stanton, J. F. Detection of the far-IR ν_{12} bending level in propargyl: A complete set of fundamentals for an important radical. *J. Phys. Chem. A* **2012**, *116*, 10338–10343.
- (58) Pullen, G. T.; Franke, P. R.; Haupa, K. A.; Lee, Y.-P.; Doublerly, G. E. Infrared spectroscopy of the n-propyl and i-propyl radicals in solid para-hydrogen. *J. Mol. Spec* **2019**, *363*, 111170.
- (59) Abeysekera, C.; Hernandez-Castillo, A. O.; Stanton, J. F.; Zwier, T. S. Broadband microwave spectroscopy of 2-furanyloxy radical: Primary pyrolysis product of the second-generation biofuel 2-methoxyfuran. *J. Phys. Chem. A* **2018**,
- (60) Johansen, S. L.; Martin-Drumel, M.-A.; Crabtree, K. N. Rotational spectrum of the β -cyanovinyl radical: A possible astrophysical N-heterocycle precursor. *J. Phys. Chem. A* **2019**, *123*, 5171–5177.
- (61) Szalay, P. G.; Vázquez, J.; Simmons, C.; Stanton, J. F. Triplet instability in doublet systems. *J. Chem. Phys.* **2004**, *121*, 7624.
- (62) Motzke, A.; Lan, Z.; Woywod, C.; Domcke, W. Simulation of the photodetachment spectrum of the pyrrolide anion. *Chem. Phys.* **2006**, *329*, 50–64.
- (63) Watson, J. K. G. Determination of centrifugal distortion coefficients of asymmetric-top molecules. *J. Chem. Phys.* **1967**, *46*, 1935.
- (64) McCarthy, M. C.; Lee, K. L. K.; Carroll, P. B.; Porterfield, J. P.; Changala, P. B.; Thorpe, J. H.; Stanton, J. F. Exhaustive product analysis of three benzene discharges by microwave spectroscopy. *J. Phys. Chem. A* **2020**, *124*, 5170–5181.

- (65) Bunker, P. R.; Jensen, P. *Molecular Symmetry and Spectroscopy*; NRC Research Press: Ontario, CA, 1979.
- (66) Bermudez, C.; Bailleux, S.; Cernicharo, J. Laboratory detection of the rotational-tunnelling spectrum of the hydroxymethyl radical, CH₂OH. *Astron. Astrophys.* **2017**, *598*, 9.
- (67) DeVine, J. A.; Babin, M. C.; Blackford, K.; Neumark, D. M. High-resolution photoelectron spectroscopy of the pyridinide isomers. *J. Chem. Phys.* **2019**, *151*, 064302.
- (68) Korte, A.; Mardyukov, A.; Sander, W. Pyridyl- and pyridylperoxy radicals – A matrix isolation study. *Aust. J. Chem.* **2014**, *67*, 1324.
- (69) Tokaryk, D. W.; Van, W. A. Fourier transform spectra of the ν_{16} , $2\nu_{16}$, and $2\nu_{16}-\nu_{16}$ bands of pyrrole taken with synchrotron radiation. *Can. J. Phys.* **2009**, *87*, 443–448.
- (70) Tokaryk, D.; Culligan, S.; Billingham, B.; van Wijngaarden, J. Synchrotron-based far-infrared spectroscopy of furan: Rotational analysis of the ν_{14} , ν_{11} , ν_{18} and ν_{19} vibrational levels. *J. Mol. Spec* **2011**, *270*, 56–60.
- (71) van Wijngaarden, J.; Van Nest, S. J.; van Dijk, C. W.; Tokaryk, D. W. Rovibrational spectrum and analysis of the ν_8 band of thiophene using infrared synchrotron radiation. *J. Mol. Spec* **2010**, *259*, 56–59.
- (72) Hrodmarsson, H. R.; Garcia, G. A.; Nahon, L.; Gans, B.; Loison, J.-C. Threshold photoelectron spectrum of the anilino radical. *J. Phys. Chem. A* **2019**, *123*, 9193–9198.
- (73) Mellouki, A.; Liévin, J.; Herman, M. The vibrational spectrum of pyrrole (C₄H₅N) and furan (C₄H₄O) in the gas phase. *Chemical Physics* **2001**, *271*, 239–266.
- (74) Nixon, C. A.; Achterberg, R. K.; Ádámkóvics, M.; Bézard, B.; Bjoraker, G. L.; Cornet, T.; Hayes, A. G.; Lellouch, E.; Lemmon, M. T.; López-Puertas, M. et al. Titan

- science with the James Webb Space Telescope. *Publ. Astron. Soc. Pac.* **2016**, *128*, 018007.
- (75) McMahon, R. J.; McCarthy, M. C.; Gottlieb, C. A.; Dudek, J. B.; Stanton, J. F.; Thaddeus, P. The radio spectrum of the phenyl radical. *Astrophys. J.* **2003**, *590*, L61–L64.
- (76) Oyama, T.; Funato, W.; Sumiyoshi, Y.; Endo, Y. Observation of the pure rotational spectra of trans- and cis-HOCO. *J. Chem. Phys.* **2011**, *134*, 174303.
- (77) Hernandez-Castillo, A. O.; Abeysekera, C.; Stanton, J. F.; Zwier, T. S. Structural characterization of phenoxy radical with mass-correlated broadband microwave spectroscopy. *J. Phys. Chem. Lett.* **2019**, *10*, 2919–2923.
- (78) Patterson, D.; Doyle, J. M. Cooling molecules in a cell for FTMW spectroscopy. *Mol. Phys.* **2012**, *110*, 1757–1766.
- (79) Porterfield, J. P.; Satterthwaite, L.; Eibenberger, S.; Patterson, D.; McCarthy, M. C. High sensitivity microwave spectroscopy in a cryogenic buffer gas cell. *Rev. Sci. Instrum.* **2019**, *90*, 053104.
- (80) Gottlieb, C. A.; Gottlieb, E. W.; Thaddeus, P. Laboratory and astronomical measurement of the millimeter wave spectrum of the ethynyl radical CCH. *Astrophys. J.* **1983**, *264*, 740–745.
- (81) Bailleux, S.; Dréan, P.; Godon, M.; Zelinger, Z.; Duan, C. First observation of the rotational spectrum of the bromomethyl radical, CH₂Br. *Phys. Chem. Chem. Phys.* **2004**, *6*, 3049–3051.
- (82) Bailleux, S.; Dréan, P.; Zelinger, Z.; Civiš, S.; Ozeki, H.; Saito, S. Millimeter wave spectrum of bromomethyl radical, CH₂Br. *J. Chem. Phys.* **2005**, *122*, 134302.



TOC Graphic